PUBLICATIONS OF THE ASTRONOMICAL SOCIETY OF THE PACIFIC, 112:1112–1120, 2000 August

A Tunable Echelle Imager

I. K. BALDRY AND J. BLAND-HAWTHORN

Anglo-Australian Observatory, P.O. Box 296, Epping, NSW 1710, Australia; baldry@aaoepp.aao.gov.au, jbh@aaoepp.aao.gov.au

Received 2000 March 13; accepted 2000 April 17

ABSTRACT. We describe and evaluate a new instrument design called a tunable echelle imager (TEI). In this instrument, the output from an imaging Fabry-Perot interferometer is cross-dispersed by a grism in one direction and dispersed by an echelle grating in the perpendicular direction. This forms a mosaic of different narrowband images of the same field on a detector. It offers a distinct wavelength multiplex advantage over a traditional imaging Fabry-Perot device. Potential applications of the TEI include spectrophotometric imaging and OH-suppressed imaging by rejection.

1. INTRODUCTION

One of the most versatile instruments for astronomical narrowband imaging is the gap-scanning Fabry-Perot (FP) etalon. Light passing through an FP produces a series of wavelength passbands called orders (examples of the transmission are shown in Fig. 1).

The positions of the passbands can be moved by varying the separation of the cavity surfaces (e.g., Atherton et al. 1981; Atherton 1995; Bland-Hawthorn & Jones 1998). However, in order to image a field with an FP, broad- or intermediate-band filters are usually used to block out the light from all the passbands except the one of interest. An alternative method is to use a dispersive element to separate the images formed by different FP orders. Recently this principle has been used in the PYTHEAS instrument (le Coarer et al. 1995) and the GraF instrument (Chalabaev & le Coarer 1995; Chalabaev, le Coarer, & le Mignant 1999a; Chalabaev et al. 1999b). In this paper, we consider the use of a cross-dispersed echelle grating[1] crossed with a gap-scanning FP called a tunable echelle imager (TEI). This forms a mosaic of narrowband images with different wavelengths on a detector, and by scanning the plate separation of the FP, a complete data cube can be obtained (two-dimensional image plus one-dimensional spectral).

1.1. The Basic Physics

The wavelength positions of the FP orders are described by the equation for constructive interference:[2]

$$m_{\rm fp}\,\lambda = 2\mu d\cos\theta\,, \tag{1}$$

where $m_{\rm fp}$ is the FP order, μ is the refractive index of the medium in the cavity gap, d is the plate separation (or gap spacing), and θ is the angle of incidence.

The bandwidth of each FP order is dependent on the reflectivity and defects of the coated surfaces (nonparallelism). The ratio between interorder wavelength spacing ($\Delta\lambda$) and the FWHM bandwidth ($\delta\lambda$) is called the effective finesse:

$$N = \frac{\Delta\lambda}{\delta\lambda}\,. \tag{2}$$

The finesse is also related to the contrast between the peak transmission of an order and the minimum transmission between orders. For contrast values greater than 100, 250, 500, or 1000, the finesse needs to be greater than 16, 25, 35, or 50, respectively. At high finesse, the efficiency can drop significantly due to defects (Atherton et al. 1981). A finesse between 20 and 40 is optimal for a high-throughput imaging FP (Bland-Hawthorn 1995).

The echelle grating (EG) disperses the FP orders using multiorder diffraction. The diffracted angle (β) for gratings that are not immersed between prisms is determined from the grating equation,

$$m_{\rm eg}\,\lambda = \mu\Lambda(\sin\alpha + \sin\beta)\,, \tag{3}$$

where $m_{\rm eg}$ is the EG order, μ is the refractive index of air, Λ is the grating period, and α is the incidence angle in air.

With an echelle grating, several wavelengths corresponding to different EG orders are diffracted at or near the same angle. For this reason, a low-dispersion element is needed to separate the EG orders. This could be another grating, one or more prisms, or a grism.

[1] We use the term "echelle" for any multiorder diffraction grating used above about the fifth order, rather than distinguishing between an "echellette" and an "echelle" grating.

[2] Note that eq. (1) does not include the effect of phase changes on reflection (Atherton et al. 1981; Jones & Bland-Hawthorn 1998). Such phase changes have a significant impact only for low-order etalons which are not considered here.

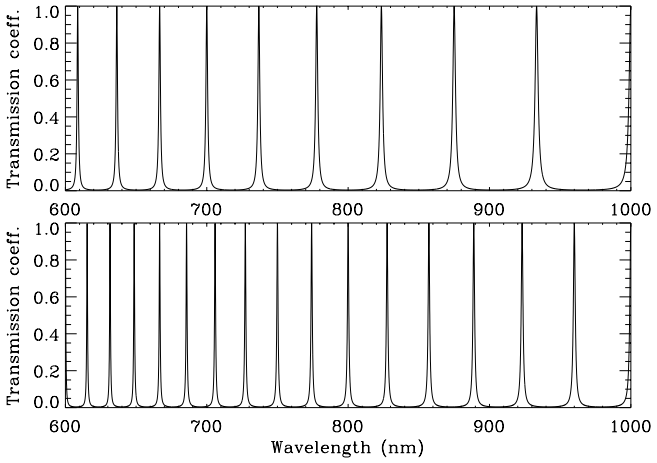

FIG. 1.—Transmission profiles for Fabry-Perot filters with gap spacings of 7.0 and 12.0 μm. The upper plot shows orders from 14 on the right to 23 on the left; the lower plot shows orders 24–40.

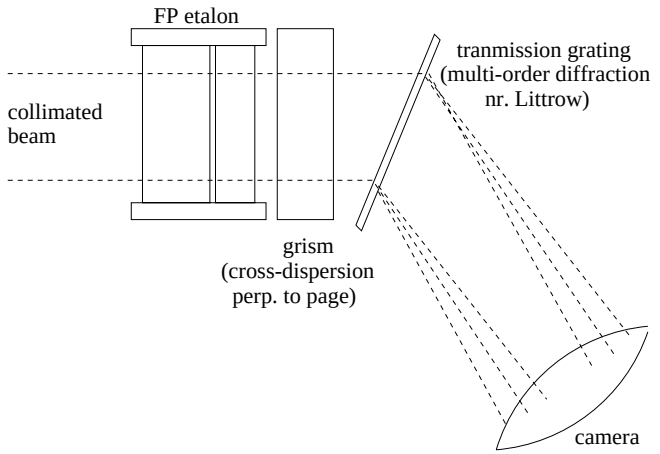

FIG. 2.—TEI with a transmission echelle grating. The grism disperses the FP orders perpendicular to the page. The echelle grating disperses the light near Littrow thus preserving the aspect ratio of the field on the detector. The many orders of the echelle allow a mosaic of images to be formed.

2. TEI SETUP

A TEI system is suitable for use at Cassegrain focus with a small collimated beam, preferably less than 100 mm in diameter for cheaper and better-quality etalons. An aperture is placed in the telescope focal plane in order to prevent overlap of images at the detector. The TEI is placed in the collimated beam. Different setups are shown in Figures 2, 3, and 4.

The first optical element is the Fabry-Perot filter, which produces a series of narrow passbands or orders. Alternatively, it is possible to put one or both of the dispersing elements before the FP. The advantage in placing the FP first is that all the light from a given point source passes through the FP at the same angle (θ). This allows for a smaller etalon, and the variations in central wavelength across a field are the same for all orders (consider the cos θ factor in eq. [1]). If the variation in θ is small enough, the image of each field will be effectively monochromatic. For monochromaticity, it is preferable that the center of the field is on-axis with the FP, i.e., to minimize the variation in cos θ.

The second optical element is a grism which separates the FP orders with low-dispersion first-order diffraction. In principle, a grating without a prism could be used. The advantage of using a grism is that it is more likely to be compatible with existing astronomical optical instruments if the beam is not deviated significantly at this point. Some grism formats are shown in Figure 5.

In some cases, it may be necessary to include a colored-glass filter to block second- and higher order diffraction by the grism. This could be placed before the FP element to minimize scattered light in the TEI.

The third optical element disperses the light in the perpendicular direction (to the grism) with high-dispersion multiorder diffraction. The dispersion is too high to correct to zero beam deviation by using a prism. The setup in Figure 2 uses a transmission grating with Littrow diffraction. The advantage of this is that the beam size remains the same after diffraction and, therefore, the pixel scale on the detector is the same as for direct imaging. The setup in Figure 3 uses a reflection grating. Higher spectral resolution (or a larger field for a given resolution) can be achieved with this setup, but there is an anamorphic increase in beam size. An alternative reflection grating setup is shown in Figure 4 with an anamorphic decrease in beam size. In this case, it may be advantageous to place the grism after the reflection grating.

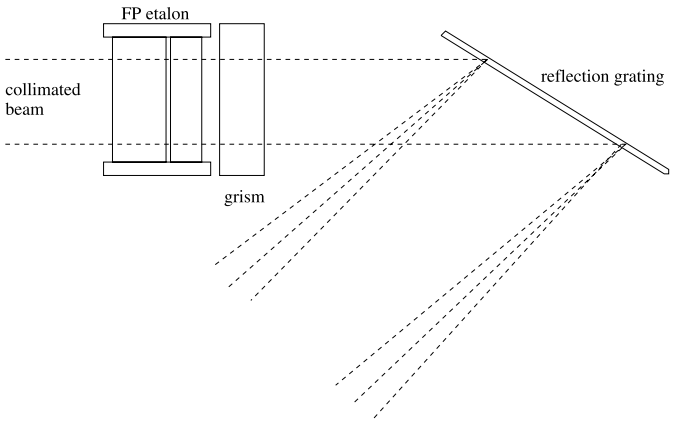

FIG. 3.—TEI with a reflection echelle grating (blaze to collimator). In this case, the echelle grating expands the beam.

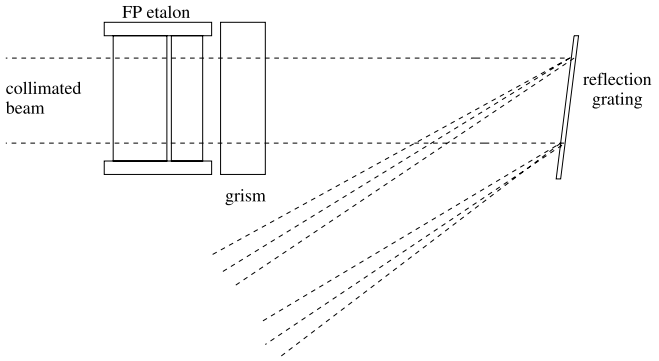

FIG. 4.—TEI with a reflection echelle grating (blaze to camera). In this case, the echelle grating reduces the size of the beam.

The use of an articulated camera[3] would allow a choice of the beam deviation that is most suitable for the experiment. Especially in the case of the transmission echelle grating, the ability to control the observed angle of diffraction allows significant control over the dispersion and anamorphic phase holographic (VPH) technology offers another advantage for the completely transmissive version of the TEI, in that the grism and echelle grating could be combined into one optical element for higher efficiency (a multiplexed grating; Barden et al. 2000).

[3] For example, articulated cameras are planned for the ATLAS (Robertson et al. 2000) and OSIRIS (Cepa et al. 2000) spectrographs.

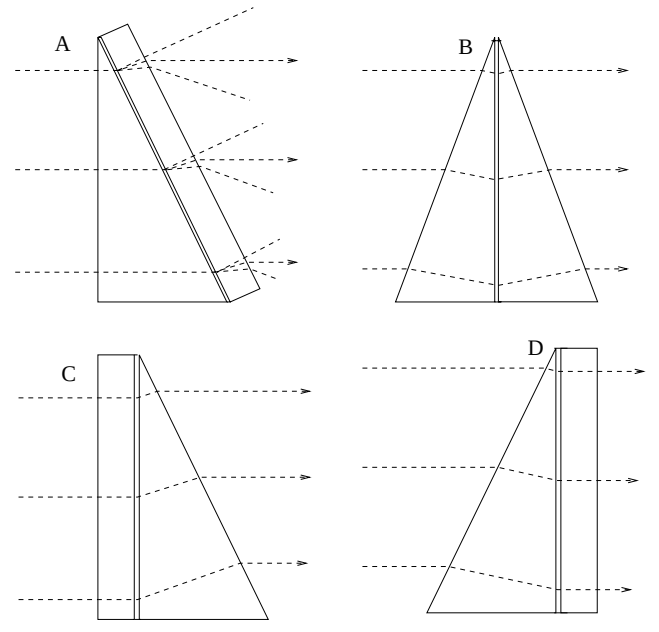

FIG. 5.—Examples of grism formats. With A- and B-type formats, the beam remains the same size for zero-deviation light. The C-type format reduces the size of the beam while the D-type format expands the beam slightly.

2.1. Parameters

There are a number of different parameters that define the properties of the instrument. The principal parameters that we will consider are as follows:

for the telescope:
- the field-of-view size,
- the beam reduction factor (collimated-beam diameter/telescope diameter $= f_{\rm coll}/f_{\rm tel}$), which determines the scaling between angles in the collimated beam and on the sky;

for the Fabry-Perot filter:
- the separation between the highly reflective surfaces of the FP (d), which determines the central wavelengths of the orders and the separations between the orders,
- the finesse (N), which determines the resolution and contrast for a given order;

for the echelle grating:
- the line density of the grating ($1/\Lambda$),
- the incident and diffracted angles (α and β);

for the grism:
- the line density of the grating,
- the angle and the refractive index of the prism(s),
- the incident and diffracted angles.

In the next section (§ 2.2), we give some examples of various setup parameters.

2.2. Examples

To determine the type of images that can be obtained with a TEI, we shall consider a system that can image a $12^\circ \times 12^\circ$ angular spread in the collimated beam. This corresponds to a $6' \times 6'$ field of view for a telescope with a beam reduction factor of 1/120 (e.g., a 10 m telescope with an 83 mm collimated beam) or a $12' \times 12'$ view with a beam reduction factor of 1/60 (e.g., a 4 m telescope with a 67 mm beam). For the $6' \times 6'$ field, the image sampling corresponds to $0\farcs18$ pixel^{-1} for a 2K $\times$ 2K detector.

Examples of various setup parameters are shown in Table 1. The fixed grism format disperses the wavelength range 600–1000 nm across the detector with first-order diffraction. For most optical systems, a colored filter would be required to block wavelengths below 500 nm (e.g., OG 550) to avoid contamination of the images with second-order

TABLE 1

EXAMPLES OF VARIOUS SETUP PARAMETERS FOR A TEI

	FABRY-PEROT PARAMETERS			ECHELLE-GRATING PARAMETERS						
APERTURE FIELD SIZE[a] (arcsec)	Plate Separation (μm)	Resolution at 600 nm[b]	No. of Orders[c]	Type[d]	Line Density (mm^{-1})	Incidence Angle (deg)	Diffraction Angle[e] (deg)	Anamorphic Factor	No. of Orders[f]	FIGURE
48 × 38	12	1200	17	T	145	25	25	1.00	5	6
39 × 23	27	2700	37	T	145	32	32	1.00	6	7
39 × 14	45	4500	61	T	145	32	32	1.00	6	...
19 × 11	80	8000	107	T	90	40	40	1.00	11	8
20 × 9	80	8000	107	R	90	25	55	0.63	10	9
20 × 14	80	8000	107	R	90	55	25	1.58	10	10
12 × 6	190	19000	254	R	70	43	63	0.62	16	11
12 × 6	310	31000	414	R	70	63	43	1.61	16	...
15 × 4	900	90000	1201	R	100	75	55	2.22	13	...

NOTE.—All the examples use a grism (type-A format, 410 lines mm^{-1}, 29° prism, $n_{prism} = 1.67$) which gives zero deviation at a wavelength of 800 nm with first-order diffraction. For the reflection echelle gratings, the angle between camera and collimator is 20° or 30°.

[a] The field size chosen to match the setup with no overlap of imaged FP orders, assuming a beam reduction factor of 1/120 (e.g., a 10 m telescope with an 83 mm collimated beam). For a beam reduction factor of 1/60 (e.g., a 4 m telescope with a 67 mm beam), the field dimensions are doubled.

[b] The resolving power ($\lambda/\delta\lambda$) at 600 nm, assuming a finesse of 30, $\theta = 0$, and $\mu = 1$ for the FP.

[c] The number of FP orders between 600 and 1000 nm.

[d] T: transmissive; R: reflective.

[e] The diffracted angle required to image on the central axis of the detector (ideally peak efficiency).

[f] The number of useful EG orders for the wavelengths between 600 and 1000 nm.

diffraction from the grism. This range was chosen to span roughly an octave in spectral coverage. The TEI setup parameters can easily be adapted for other wavelength ranges, beam characteristics, and detector sizes.

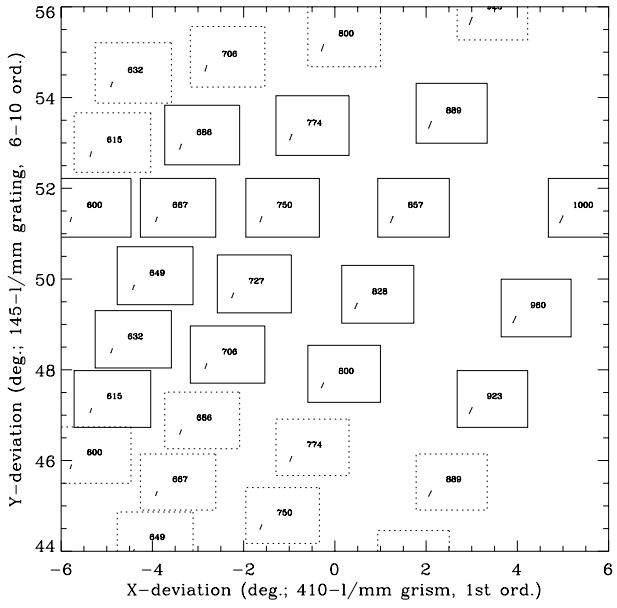

FIG. 6.—Mosaic of images produced by a TEI ($d = 12$ μm). The angles relate to deviations within the collimated beam (not to angles on the sky). The central wavelengths in nanometers of each narrowband image are shown within each square. Images shown with dashed lines are repeated FP orders. The line in the bottom-left corner of each image is the PSF (2 times the FWHM in length) caused by the dispersion.

The plate separation of the FP determines the number of imaged orders between 600 and 1000 nm. This combined with the finesse determines the resolving power of the instrument. If the finesse is constant across the observed wavelengths, then the resolving power will be highest at the shortest wavelength and proportional to $1/\lambda$. This could be

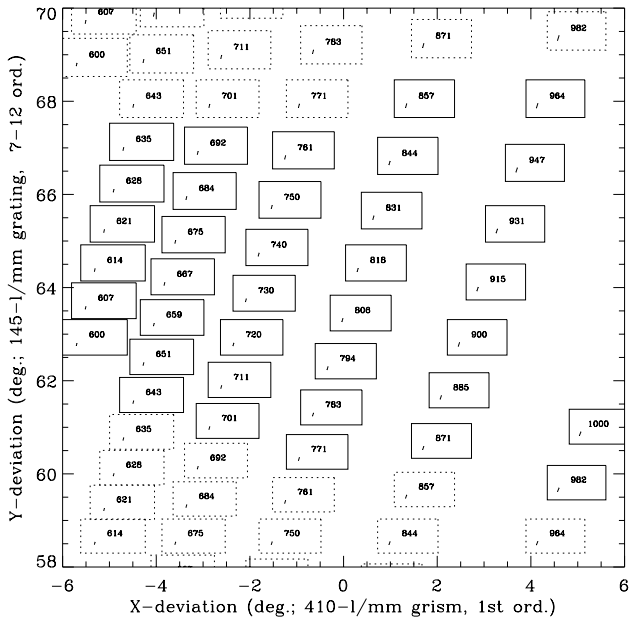

FIG. 7.—Mosaic of images produced by a TEI ($d = 27$ μm)

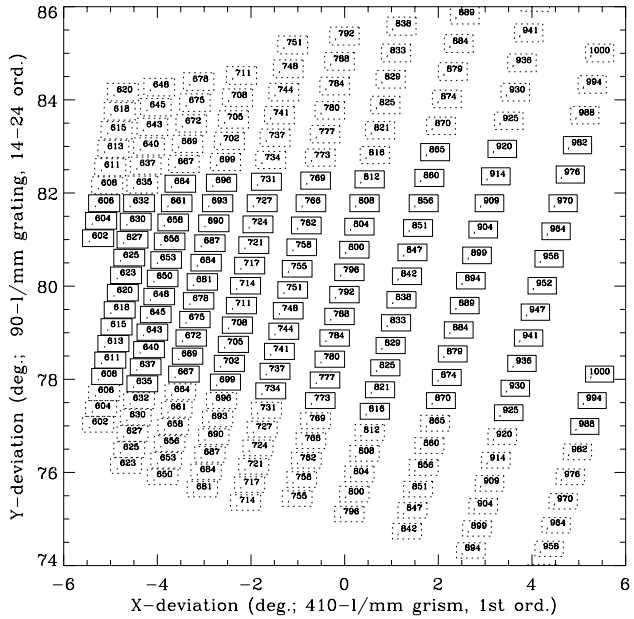

FIG. 8.—Mosaic of images produced by a TEI ($d = 80\ \mu$m)

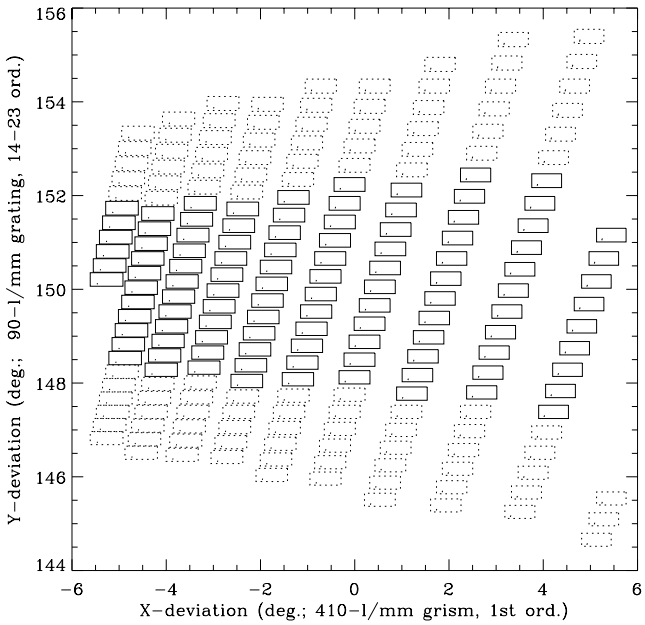

FIG. 10.—Mosaic of images produced by a TEI ($d = 80\ \mu$m)

altered by increasing the reflectivity as a function of wavelength.

The parameters of the echelle grating determine the maximum aperture size usable at a given resolving power (without overlap of FP orders). Higher dispersion gratings and/or increased anamorphic factor allow for wider apertures or a larger resolving power. The maximum length of the aperture is determined by the separation of the EG orders imaged onto the detector. Simulated images of FP orders with various EG orders and dispersions (Table 1) are shown in Figures 6–11.

3. DISCUSSION

3.1. Observing and Data Reduction

To fully sample the spectral dimension at the resolving power of the TEI setup, it will be necessary to take a

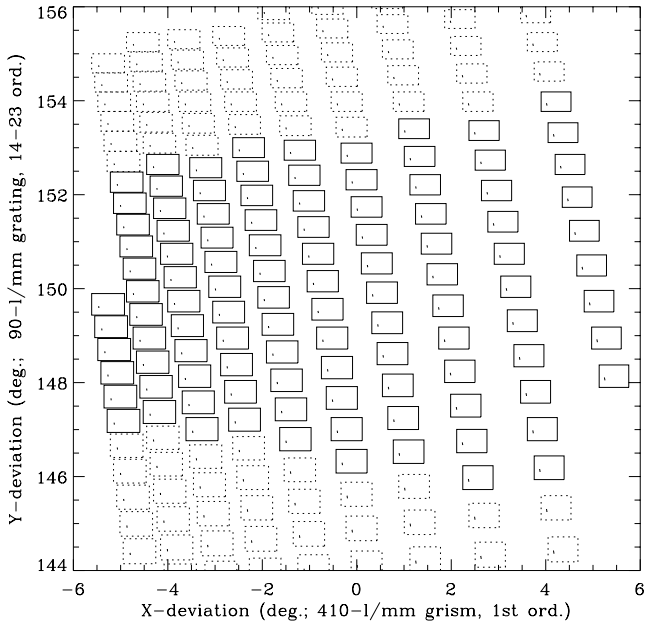

FIG. 9.—Mosaic of images produced by a TEI ($d = 80\ \mu$m)

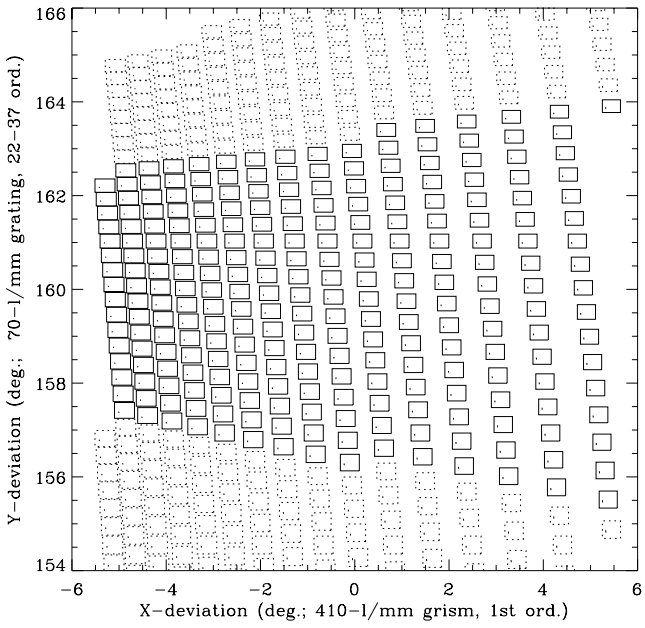

FIG. 11.—Mosaic of images produced by a TEI ($d = 190\ \mu$m)

number of exposures (at different FP gap spacings) equal to or greater than the finesse of the FP. The reason for a greater number of exposures is because the requirements for sampling at the shortest wavelength may be different from those at the longest wavelength. In many cases, there will be double sampling of some wavelengths near the shortest wavelength; these could be used as a self-calibration check in reconstructing the spectral dimension.[4] Spectrophotometric measurements could be obtained in photometric conditions by calibrating with a standard star.

The TEI can mimic a true three-dimensional spectrograph by scanning, as described above. Some applications may not need scanning or need only partial scanning (a few exposures) if the sampling of the spectral dimension is adequate. For example, multiple narrowband imaging could be used to selectively combine images in order to suppress sky-emission lines, thus mimicking an OH-suppression instrument.

Wavelength calibration of a TEI would be made using arc lamps to define the wavelength for each order and gap spacing for the etalon. The calibration is then uniquely defined for a given gap spacing and should be stable during an exposure using capacitance micrometry (Hicks, Reay, & Atherton 1984). Advantageously, the spectral stability of the TEI is not subject to instrument flexure as with a normal Cassegrain spectrograph.

In some of the example image formats, it appears that optimal use is not made of the detector in the sense that there are repeated orders (e.g., Fig. 10). However, if every order is repeated twice on the detector, it may increase the efficiency and allow the possibility of removing image defects (e.g., hot pixels, cosmic rays, bad columns) by comparing the same narrowband image.

3.2. Aperture Width and the PSF

The dispersion of the gratings spreads out the light from a single FP order, contributing to the point-spread function (PSF) of the image. The FWHM of this one-dimensional contribution is equal to the separation (on the detector) between adjacent FP orders divided by the finesse. The lines in the bottom left corner of each image in Figures 6–11 represent this PSF.

If the aperture size is maximized for a particular echelle grating and FP setup, then the FWHM of the dispersive PSF is equal to the width of the aperture divided by the finesse, for the lowest wavelength. Therefore, if a certain image resolution is required in both spatial dimensions (the TEI only degrades resolution in one direction), then there is a limit on the setups to those with certain aperture widths. For example, in the case of adaptive optics, a resolution of 0.″1 may be required, limiting the aperture width to 3″ (with a finesse of 30). Alternatively, if 0.″5 is satisfactory, then an aperture width of 15″ would be suitable. If good image resolution is required in only one direction, then the aperture width can be larger still.

We note that the elongated PSF is a common occurrence in radio interferometry where many software tools exist to treat such data (Perley et al. 1994). The TEI situation is somewhat better because an instrument rotation allows us to sample the field with orthogonal PSF orientations.

3.3. Anamorphic Factor

The ratio of the beam sizes after and before diffraction by a grating is called the anamorphic factor. For a reflection grating or a transmission grating without prisms, the anamorphic factor

$$A = \frac{\cos \beta}{\cos \alpha}, \tag{4}$$

where α and β are the incident and diffracted angles in air. The change in beam size is inverse to the change in angular size (the angle between light rays in the collimated beam). A grating setup which has an anamorphic factor above unity can increase the resolution because the angular size of the aperture (in the dispersion direction) is reduced. However, the increase in resolution is less than the anamorphic factor because the dispersion is also reduced (though not by as much).

Figures 9 and 10 show the effect of varying the anamorphic factor with the same resolution and EG orders (see Table 1). Larger apertures can be used with the blaze-to-collimator setup (increasing beam size) even though the images appear smaller on the detector (Fig. 10). Using the example of a 2K × 2K CCD and a 6′ × 6′ field, the pixel sampling on the detector would change from 0.″18 to 0.″28 pixel^{-1} across the width of the aperture (14″). The change in sampling is not critical in this case because the dispersion PSF is about 0.″47 (FWHM). In quadrature with 0.″5 seeing, we find that the sampling is still adequate. In other cases a large anamorphic factor could cause undersampling of the PSF (instrumental and seeing) on the detector. Ideally, the change in sampling caused by an increase in beam size could be matched to the decrease in image resolution. A decrease in beam size cannot cause undersampling on the detector.

With a limited number of gratings, it would be useful to be able to use either a transmission or a reflection grating setup, with an increase or decrease in beam size. In this way, the aperture width could be matched more easily to the desired spectral resolving power.

[4] Bland & Tully (1989) noted that it was easier to reconstruct the λ-dimension than an image dimension (e.g., as with a scanning slit or IFU).

A decrease or no change in beam size after dispersion has the advantage of instrumental compactness, in that the camera optics could be smaller than if an increase in beam size is allowed.

Note that the peak efficiency of an EG order decreases away from Littrow approximately proportional to A^2 or $1/A^2$ (for $A < 1$ or $A > 1$, respectively) with the light being shifted to off-blaze orders (Bottema 1981). Some of the efficiency loss can be recovered with imaging of the off-blaze light. However, a TEI will generally be more efficient if the anamorphic factor is chosen to be nearer to unity that the reflection grating examples given in Table 1.

3.4. Finesse

Choosing the finesse is a trade-off between a number of factors. A lower finesse has the advantage of needing fewer scans to complete the data cube. In effect, the total throughput of the instrument is approximately proportional to $1/N$. A higher finesse has the advantage of higher spectral and image resolution, and better suppression of the light between the narrow bands.

3.5. Comparison with a Mono-Order FP

The advantages of the TEI over an FP, where a single order has been selected with a blocking filter, include imaging in many narrow bands simultaneously and imaging at any wavelength and spectral resolution without the need for many order-sorter filters. The disadvantages include a smaller field of view, compromised image resolution (in one direction) because of the PSF caused by the dispersion, and efficiency loss for a single order due to the extra dispersive elements.

A significant aspect of the TEI is that the field, although smaller, will be monochromatic or nearly monochromatic in many cases. In fact, the size of the field decreases as the spectral resolving power (R) is increased which is in the same sense as the Jacquinot (1954, 1960) criterion for a monochromatic field:

$$R\Omega = 2\pi\,, \tag{5}$$

where Ω is the solid angle at the FP. The TEI parameters can be chosen to give maximum spectral coverage for the monochromatic field.

3.6. Comparison with the GraF Concept

The GraF concept uses a single dispersive element to separate the FP orders (Chalabaev & le Coarer 1995). Such a concept has been used in the GraF/ADONIS instrument on the ESO 3.6 m telescope (Chalabaev et al. 1999a, 1999b). This instrument operates in the near-IR with adaptive optics used to obtain 0.″1 image resolution. As an example, it can provide 10 images of $9'' \times 0.''9$ in the H band at a spectral resolution of 10,000 (Chalabaev et al. 1999b). The field is thus small and narrow for high image resolution.

Here, we compare the TEI with a more general GraF instrument. A lower image resolution GraF instrument could, for example, have a field of $6' \times 20''$.

The advantage of the TEI is the ability to image in more FP orders simultaneously, i.e., providing a larger wavelength coverage except for the lowest spectral resolutions. The disadvantages include efficiency losses due to the extra dispersive element and a shorter field of view.

In general, the shorter field of view is not a significant disadvantage because (i) the field will not be monochromatic over a longer field of view and (ii) astrophysical objects of interest may not be extended in one direction only, over the length of field possible with a GraF instrument (arcminutes).

The TEI could be converted to a GraF instrument by replacing the echelle grating with a mirror or positioning the camera for direct imaging.

3.7. Comparison with an Echelle Grating

The advantages of the TEI over a standard echelle grating include imaging and better spectrophotometry because a wider aperture can be used without compromising wavelength calibration or resolution. A disadvantage is that it requires scanning (tens of exposures) to fully sample a wavelength region.

The TEI can reach the same resolution as a standard echelle with a wider aperture and a smaller beam. The first factor allows better sampling of extended sources, and the second allows the TEI to be a Cassegrain instrument with a smaller camera. These two factors partially offset the disadvantage of the scanning requirement in terms of efficiency. In certain cases, the TEI could be comparable to a slit echelle spectrograph for high-resolution spectroscopy of extended sources. For spectrophotometry and imaging, the TEI is significantly better.

3.8. Comparison with an IFS

In recent years, there has been great interest in the use of integral-field spectrographs (IFS). These include image slicers (e.g., Content 2000), integral-field units, and the TIGER approach (Courtès 1982; Courtès et al. 1988; Bacon et al. 1995). Both TEI and IFS instruments are true three-dimensional spectrographs. However, they differ in one key respect. For the IFS, the incident wave front is divided and dispersed, in contrast to the TEI where the wave front is only dispersed.

The advantages of the TEI compared to an IFS include better imaging and spectrophotometry because images do not need to be reconstructed, a larger field of view for a

given detector size, and potentially higher spectral resolution. The disadvantages include the scanning requirement to fully sample a wavelength region and compromised image resolution (in one direction) because of the PSF.

Integral-field spectrographs divide the focal plane, and therefore image integrity can be compromised (i.e., they are not spectrophotometric). So while an IFU is more efficient than a TEI device, for the same image size and spectral resolution requirements, there are certain cases where the TEI's undivided approach to three-dimensional spectroimaging could be more beneficial.

3.9. Some Applications

The potential applications include spectroimaging and/or high-resolution spectroscopy of extended sources, through production of a full data cube, OH suppression in the 600–1600 nm wavelength range (*RIzJH*), and targeted line imaging.

The OH-suppression method is to selectively combine the images produced by a TEI, rejecting those images that contain OH-line emission (or applying a lower weight). This will considerably reduce the sky background especially in the *J* and *H* bands. Figure 12 shows an example of an FP transmission profile plotted over the *J*-band sky emission spectrum.

Evaluation of OH-suppression methods has been done by Herbst (1994), Jones, Bland-Hawthorn, & Burton (1996), and Offer & Bland-Hawthorn (1998). Equation (5) of Jones et al. (1996) gives the gain (G) in performance of an OH-suppression filter for the broadband signal-to-noise ratio (S/N).[5] For background-limited conditions, this equation reduces to

$$G = \frac{\tau}{\sqrt{\beta}}, \tag{6}$$

where τ is the fraction of object flux remaining and β is the fraction of background remaining. Simple numerical calculations, for the broadband S/N in the *J* band, show that G can be larger or about unity, when selectively combining TEI images at resolving powers of above 10,000 using a finesse of 30. Note that this broadband gain applies only to dark time because the TEI is imaging between the OH lines where the background flux is moon-phase dependent. Additionally, a suitable TEI instrument could image in the *J* and *H* bands simultaneously and provide a spectrum (low resolution if the FP is not scanned).

[5] The analysis of Jones et al. (1996) uses Poisson-noise statistics. They point out that even $G \sim 1$ could provide a significant S/N gain, if most of the OH emission is removed from the background, because the continuum background is more stable and therefore systematic effects could be reduced.

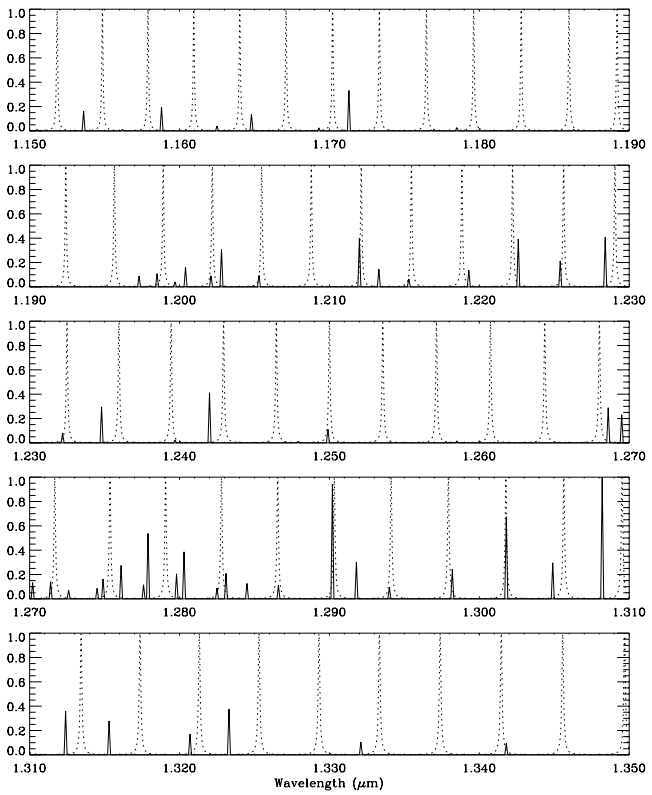

FIG. 12.—Plots of the transmission profile of an FP (*dotted line*) with a gap spacing of 220 μm and a finesse of 30, and an OH sky emission spectrum (*solid line*), in the *J* band. The TEI images produced by the different FP orders can be combined selectively to exclude most of the OH emission. The sky emission spectrum is the same as that used by Offer & Bland-Hawthorn (1998).

As with a mono-order FP, the TEI could be used for targeted line imaging, but, in addition, the TEI can simultaneously provide an OH-suppressed broadband image using the nontargeted FP orders. The reduction of field of view in comparison with a standard FP mode is not always significant because, if the FP is not scanned, it is only the monochromatic field of view that images the targeted emission line.

4. SUMMARY

The tunable echelle imager offers an interesting reformation of existing spectrographs, by the use of a Fabry-Perot filter crossed with an echelle grating. This forms a mosaic of narrowband images on a detector, offering a significant multiplex wavelength advantage over a mono-order FP system.

The TEI instrument is placed in the collimated beam and includes an FP element, a grism, and an echelle grating. Parameters such as the plate separation of the FP and the dispersion of the echelle determine the resolving power and the field-of-view size of the images. Resolving powers

ranging from about 1000 to 100,000 are observable with fields of view ranging from an arcminute down to arcseconds in size.

The potential of the TEI includes its spectrophotometric integrity for producing a three-dimensional data cube and the ability to create an OH-suppressed image by selectively combining different FP orders.

We would like to thank Brian Boyle, Ted Gull, David Lee, and Keith Taylor for discussions.

REFERENCES

Atherton, P. D. 1995, in ASP Conf. Ser. 71, Tridimensional Optical Spectroscopic Methods in Astrophysics, ed. G. Comte & M. Marcelin (San Francisco: ASP), 50
Atherton, P. D., Reay, N. K., Ring, J., & Hicks, T. R. 1981, Opt. Eng., 20, 806
Bacon, R., et al. 1995, A&AS, 113, 347
Barden, S. C., Williams, J. B., Arns, J. A., & Colburn, W. S. 2000, in ASP Conf. Ser. 195, Imaging the Universe in Three Dimensions, ed. W. van Breugel & J. Bland-Hawthorn (San Francisco: ASP), 552
Bland, J., & Tully, R. B. 1989, AJ, 98, 723
Bland-Hawthorn, J. 1995, in ASP Conf. Ser. 71, Tridimensional Optical Spectroscopic Methods in Astrophysics, ed. G. Comte & M. Marcelin (San Francisco: ASP), 369
Bland-Hawthorn, J., & Jones, D. H. 1998, Publ. Astron. Soc. Australia, 15, 44
Bottema, M. 1981, Proc. SPIE, 240, 171
Cepa, J., et al. 2000, Proc. SPIE, 4008, in press
Chalabaev, A., & le Coarer, E. 1995, in Science with the VLT, Poster Paper Suppl., ed. J. R. Walsh & I. J. Danziger (Garching: ESO), 135
Chalabaev, A., le Coarer, E., & le Mignant, D. 1999a, in ASP Conf. Ser. 188, Optical and Infrared Spectroscopy of Circumstellar Matter, ed. E. Guenther, B. Stecklum, & S. Klose (San Francisco: ASP), 315
Chalabaev, A., le Coarer, E., Rabou, P., Magnart, Y., Petmezakis, P., & le Mignant, D. 1999b, in ESO Conf. and Workshop Proc. 56, Astronomy with Adaptive Optics, ed. D. Bonacicni (Garching: ESO), 61
Content, R. 2000, in ASP Conf. Ser. 195, Imaging the Universe in Three Dimensions, ed. W. van Breugel & J. Bland-Hawthorn (San Francisco: ASP), 518
Courtès, G. 1982, in IAU Colloq. 67, Instrumentation for Astronomy with Large Optical Telescopes, ed. C. M. Humphries (Dordrecht: Reidel), 123
Courtès, G., Georgelin, Y., Monnet, R., Bacon, G., & Boulesteix, J. 1988, in Instrumentation for Ground-Based Optical Astronomy, ed. L. B. Robinson (New York: Springer), 266
Herbst, T. M. 1994, PASP, 106, 1298
Hicks, T. R., Reay, N. K., & Atherton, P. D. 1984, J. Phys. E, 17, 49
Jacquinot, P. 1954, J. Opt. Soc. Am., 44, 761
———. 1960, Rep. Prog. Phys., 23, 267
Jones, D. H., & Bland-Hawthorn, J. 1998, PASP, 110, 1059
Jones, D. H., Bland-Hawthorn, J., & Burton, M. G. 1996, PASP, 108, 929
le Coarer, E., Bensammar, S., Comte, G., Gach, J. L., & Georgelin, Y. 1995, A&AS, 111, 359
Offer, A. R., & Bland-Hawthorn, J. 1998, MNRAS, 299, 176
Perley, R. A., Schwab, F. R., & Bridle, A. H., eds. 1994, ASP Conf. Ser. 6, Synthesis Imaging in Radio Astronomy (San Francisco: ASP),
Robertson, J. G., Taylor, K., Baldry, I. K., Gillingham, P. R., & Barden, S. C. 2000, Proc. SPIE, 4008, in press